Influence of the Jahn-Teller effect on the high-pressure induced phase transition of $[C(NH_2)_3]Cu(HCOO)_3$

Eduardo Suengas Rodríguez
Tutor: Javier Ruiz Fuertes

November 2024

Abstract

An investigation was made on the pressure-induced structural phase transition of the hybrid perovskite $[C(NH_2)_3]Cu(HCOO)_3$ and the influence of the Jahn-Teller (JT) effect on it. Single-crystal X-ray diffraction experiments were conducted up to 3.55 GPa. Up to 3.5 GPa, the orthorhombic ambient structure ($Pna2_1$) remains stable. At higher pressure, a monoclinic phase ($P2_1/c$) emerges, marked by distinct changes in the lattice parameters. The JT distortion decreases with increasing pressure up to a critical value of 0.32 $\AA$ but reemerges at the phase transition correlating with structural modifications and the stabilization of octahedral symmetry in $Cu-O$ bonds. The comparison with similar Cu^{2+} bearing hybrid perovskite compounds or even inorganic compounds shows a similar trend in systems with Cu^{2+}: The JT distortion decreases with pressure until it reaches a minimum value before the phase transition occurs and the JT distortion rises again. This fact evidences that keeping the breaking of the degeneracy of the d-orbitals controls the stability of the whole structure in Cu^{2+} bearing systems.

1 Introduction

Metal-organic frameworks (MOFs) including transition metals normally form hybrid perovskites with the general formula ABX_3. These materials in which B is a metal and A and X are organic molecules have attracted significant interest due to their remarkable electromagnetic properties as supermagnetism and ferroelectricity [1, 2]. The coexistence of both magnetism and ferroelectricty in these materials appears when the transition metal presents an incomplete filling of its d orbitals. Consequently, understanding the configuration and behavior of these d orbitals when the material is subjected to extreme conditions is essential when studying such properties.

One key mechanism influencing the d orbitals is the Jahn-Teller (JT) effect. This effect breaks the degeneracy of the d orbitals when the transition metal presents d^4 or d^9 electronic configurations and it is introduced into a crystal field, leading to asymmetries in the bonding of the d orbitals. For instance, in octahedral coordination environments such as those found in perovskites, the JT distortion arises particularly in systems where transition metals like Cu^{2+} exhibit a d^9 electronic configuration. This configuration leads to instability in a perfectly symmetric octahedral field, causing elongation or compression along specific axes. The ability to determine how these bonds vary under different conditions is critical to gaining a deeper understanding of the properties of these hybrid perovskites.

The crystal structure of Cu^{2+} bearing hybrid perovskites has been previously studied at high pressure in formates ($HCOO^-$). It is known that dimethylammonium copper formate $[(CH_3)_2NH_2]Cu(HCOO)_3$ undergoes a structural phase transition at 5.2 GPa to preserve the JT distortion [3, 4] and interestingly it involves an orbital reordering to cope with the JT instability.

In this work, the evolution of the crystal structure of guanidinium copper formate $[C(NH_2)_3]Cu(HCOO)_3$ is studied under compression. At room temperature, its structure is solved into $Pna2_1$ orthorhombic space group (SG). The Cu^{2+} ions are sixfold coordinated, forming CuO_6 octahedra.

Due to the JT effect, the axes of these octahedra have unequal lengths forming a pseudo D_{4h} elongated symmetry with alternated chains expanding along [100] aligning the two Cu-O long axes along the [101] and $[\bar{1}0\bar{1}]$ directions (Fig. 1). This local distortion only present in the copper guanidinium formate lowers the overall symmetry from rhombohedral $R\bar{3}c$ space group present

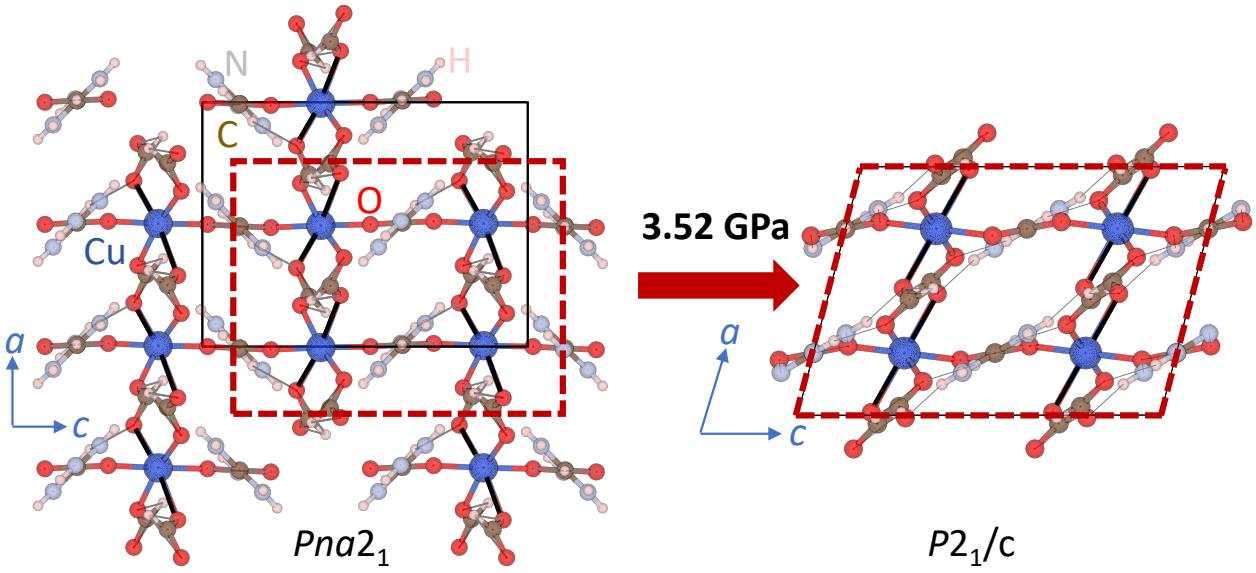

Figure 1: Crystal structures of the low-pressure (left) orhtorhombic and high-pressure (right) monoclinic phases of $[C(NH_2)_3]Cu(HCOO)_3$. The black continuous frame indicates de unit cell. The discontinuous red frames indicate how the high-pressure structure relates to the low-pressure one. The long Cu-O bonds are represented in black.

in $(NH_2)_3]M(HCOO)_3$, where M = Mn, Fe, Co, Ni, Cu, and Zn [5] to $Pna2_1$. Interestingly, the $Pna2_1$ space group belongs to the category of polar orthorhombic symmetries, which is often associated with ferroelectric or piezoelectric properties. These attributes, combined with the pressure-induced distortions in the lattice, may influence the electromagnetic behavior of the material. Under pressure, the material may also undergo a phase transition, driven in part by the JT effect. By comparing these observations with results from those obtained in the dimethylammonium counterpart, the role of the JT effect in copper formates can be further clarified, offering a deeper understanding of its impact on the structural and electromagnetic properties of the material.

2 Experimental section

The details about the synthesis of the $[C(NH_2)_3]Cu(HCOO)_3$ sample can be found in [5]. 0.02 mol of $(CH_5N_3)2{\cdot}H_2CO_3$ and 0.02 mol of HCOOH were dissolved in a stoichiometric ratio in 500 mL of bidistilled water. The solution was then mixed with a solution of 0.02 mol of $Cu(COOH)_2$ in 500 mL of water and stirred. At the end, 5 mL of ethylene glycol was added to the solution to improve the quality of the obtained crystals. After 2 weeks, transparent crystals with dimensions from 3 to 5 mm were grown at about 295 K from aqueous solution. The high-pressure single crystal x-ray diffraction (SXRD) experiments were performed in a Rigaku SuperNOVA diffractometer at the Universidad de La Laguna using Mo radiation (= 0.7107 $\AA$) placing the sample at a distance of 62 mm from the CCD detector. The data integration was carried out with the CrysAlisPro [6] software and the structural solution and refinements were performed with the Shelx package [7]. To increase pressure the sample was loaded in a Mini-Bragg diamond anvil cell (DAC) equipped with two 500 μm culet diamonds. The total opening of the DAC was 85°. The sample was loaded in between both diamonds in the cavity formed by a 200 hole performed in a 75 μm-thick preindented stainless steel gasket. The pressure transmitting medium was either a solution of methanol-ethanol (4:1) or parabar (polymerized oil). Pressure was obtained by the luminescence of a small ruby [8] sphere placed in the pressure chamber.

3 Results and Discussion

Experiments were conducted within the pressure range of 0 to 4 GPa since the diffraction power ot the sample deteriorated above this pressure. The ambient structure remained stable up to 3.5 GPa. However, at 3.52 GPa, a deviation in the angle β from 90° to 104.44(17)° was observed. This change, accompanied by the abrupt shifts in the

Table 1: Unit-cell parameters a, b, c (in Å) and their errors, β, V (Å^3), $V_{\rm oct}$, and the Jahn-Teller distortion σ_{JT} according to Eq. 1 as a function of pressure P (in GPa).

P (GPa)	0.00	0.37	0.70	1.40	2.22	2.90	3.55	3.52
SG	$Pna2_1$	$Pna2_1$	$Pna2_1$	$Pna2_1$	$Pna2_1$	$Pna2_1$	$Pna2_1$	$P2_1/c$
a **(Å)**	8.5290(3)	8.4192(11)	8.3385(12)	8.2177(9)	8.0857(12)	8.0027(11)	7.9102(4)	8.0100(7)
b **(Å)**	9.0369(3)	8.9980(16)	9.0058(17)	8.9864(9)	8.9320(13)	8.9555(13)	8.9285(6)	8.8207(15)
c **(Å)**	11.358(4)	11.328(9)	11.272(11)	11.177(7)	11.125(9)	11.020(8)	11.005(4)	11.340(30)
β **(°)**	90.000	90.000	90.000	90.000	90.000	90.000	90.000	104.44(17)
V **(Å^3)**	875.43(5)	858.16(7)	846.47(9)	825.39(5)	803.46(7)	789.78(6)	777.24(3)	775.90(22)
$V_{\rm oct}$ **(Å^3)**	12.212	12.069	11.914	11.835	11.443	11.503	11.311	11.832
σ_{JT} **(Å)**	0.4559(13)	0.4291(12)	0.4129(12)	0.3990(12)	0.3592(10)	0.3388(10)	0.3283(9)	0.4174(12)

unit cell parameters a, b and c, as illustrated in Figure 2, indicates a structural phase transition at this pressure.

The initial structure was refined in the orthorhombic space group $Pna2_1$, with cell parameters $a = 8.5290(3)$ Å, $b = 9.0369(3)$ Å, $c = 11.3581(4)$ Å, and $V = 875.43(5)$ Å^3 in very good agreement with literature [5]. Upon compression, the unit-cell parameters and volume decrease progressively. However, following the phase transition at 3.52 GPa, this smooth reduction is disrupted: the c axis experiences a sudden increase, while b axis decreases sharply. Despite these changes, the unit-cell volume continues its downward trend as expected under compression. In the new structural phase, the refined cell parameters at 3.52 GPa are $a = 8.010(7)$ Å, $b = 8.8207(15)$ Å, and $c = 11.34(3)$ Å, $\beta = 104.44(17)°$, and $V = 775.7(19)$ Å^3 as shown in Figure 2. Interestingly, the expansion of the c axis is compensated by the contraction of the a and b axes together with the distortion of the lattice and the unit-cell volume only contracts around 0.2 % (Fig. 3).

The obtained lattice parameters and unit-cell volume are collected in Table 1. The difference in compressibility between the three orthorhombic axes can be observed in Fig. 2 with the a and c axes being much more compressible than the b axis. The axial compressibilities k_a, k_b, and k_c, can be obtained using a third-order BM EOS fit if one considers a pseudocubic cell with volume $V = x^3$ and $k_x = -1/(3B_0)$ where x stands for each lattice parameter. The a ($K_a = -0.009$ GPa^{-1}) and c ($K_c = -0.004$ GPa^{-1}) axes show a large compressibility. In particular, the compressibility of the a axis is the one controlling most of the compressibility of the unit-cell. However, the compressibility of the b ($K_b = -0.001$ GPa^{-1}) axis is similar to that found in an inorganic compound. This shows the difficulty to compress the guanidinium complexes which align along the [010] direction.

After obtaining the compressibility of the three crystallographic axes we can obtain how the unit-cell volume changes under compression. The pressure dependence of the unit-cell volume can be obtained by fitting the data to a Birch-Murnaghan equation of state (EOS) [9, 10]. The result of the fit can be observed in Fig. 3 (a). In order to determine the order of the equation of state we have performed a plot of the normalized pressure (F) as a function of the Eulerian strain (f). The result is shown in the inset of Fig. 3 (b). The sign of the $\partial F/\partial f > 0$ indicates that the order of the Birch-Murnaghan equation is 3. Hence, the ambient pressure volume, the bulk modulus, and the first derivative of the bulk modulus are: $V_0 = 875.43(6)$ Å^3, $B_0 = 17.9(9)$ GPa, and $B_0' = 9.2(1.1)$. The value obtained for the bulk modulus indicates the high compressibility of the $[C(NH_2)_3]Cu(HCOO)_3$ even compared to the bulk modulus $B_0 = 24.4(4)$ GPa of the dimethilamonium counterpart [4] $[(CH_3)_2NH_2]Cu(HCOO)_3$.

At ambient pressure the Cu-O bonds of the CuO_6 octahedra of $[C(NH_2)_3]Cu(HCOO)_3$ are in Å: 1.982(7), 1.967(4), 1.953(4), 2.012(8), 2.355(4), and 2.386(4). Even though the O-Cu-O angles cannot be neglected it is reasonable to understand the compression mechanism just considering the bond distances (Fig. 1. The evolution of the averaged two long Cu-O distances and the averaged four short Cu-distances is depicted in Fig. 4 (a). All the distances reduce under compression but the long ones compress significantly faster under increasing pressure. This fact contributes substantially to a decrease of the JT distortion σ_{JT} defined in Eq. 1 and depicted as a function of pressure in Fig. 4 (b). In fact σ_{JT} goes from 0.45 to 0.34 Å just before the phase transition considering that R_{Cu-O} are the six Cu-O distances and $\langle R_{CuO} \rangle$ is the average Cu-O distance.

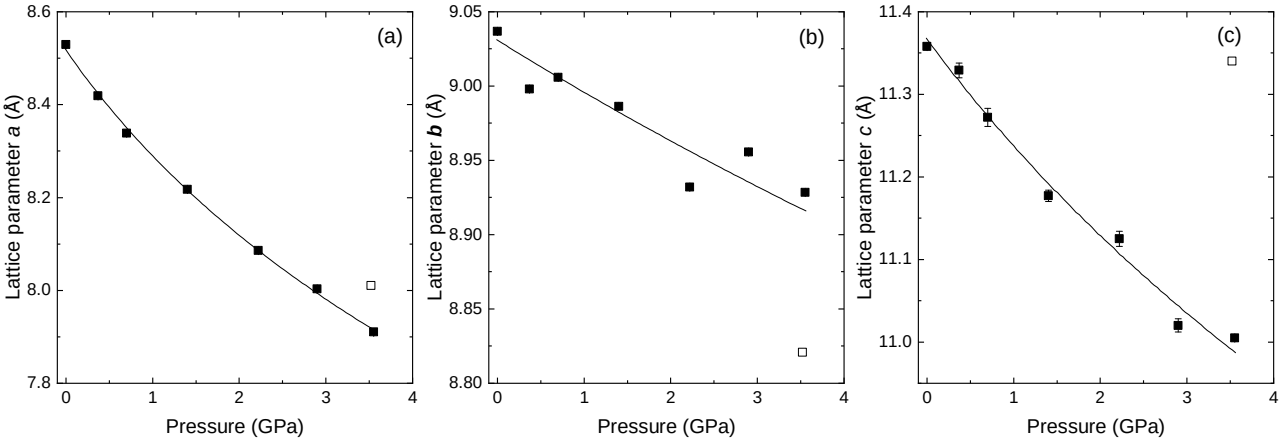

Figure 2: Pressure dependence of the lattice parameters (a) a, (b) b, and (c) c. The continuous lines are fits to a third order Birch-Murnghan equation of state. Black squares belong to the low-pressure phase while the hollow dots belong to the high-pressure phase.

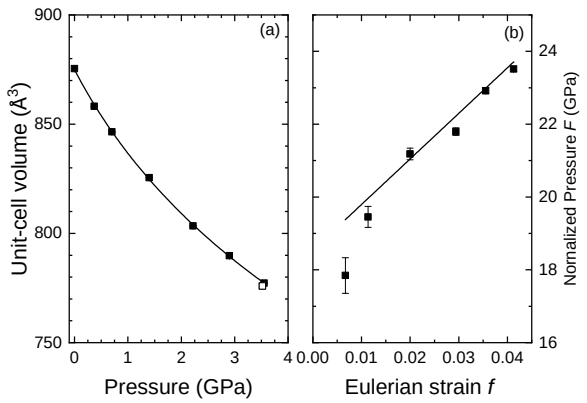

Figure 3: (a) Variation of the unit-cell volume V as a function of pressure and (b) variation of the Normalized pressure F as a function of the Eulerian strain f. The continuous lines are fits to a third order Birch-Murnaghan equation of state and a linear fit, respectively. The hollow point corresponds to the high-pressure phase.

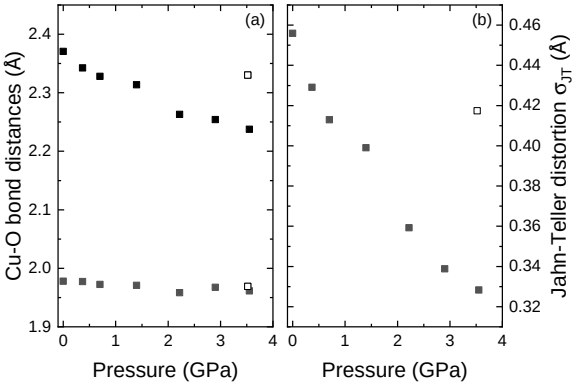

Figure 4: (a) Pressure dependence of the averaged 2 long and 4 short Cu-O bonds of the CuO_6 octahedra. (b) Pressure evolution of the Jahn-Teller distortion σ_{JT} as defined in eq. 1. The hollow point corrsponds to the high-pressure phase.

$$\sigma_{JT} = \sum_{n=1}^{6} (R_{Cu-O} - \langle R_{Cu_O} \rangle^2)^{1/2} \qquad (1)$$

The large JT distortion reduction of 24.4% in only 3.5 GPa in $[C(NH_2)_3]Cu(HCOO)_3$ (B_0 = 17.(9) GPa) means that in this compound the surrounding organic part does not serve as a shield for the CuO_6 polyhedra which directly feel the effect of pressure in their bonds. On the contrary, it is necessary to go to 10 GPa to find a similar JT distortion reduction (27%) in the CuO_6 polyhedra of inorganic $CuWO_4$ (B_0 = 139(6) GPa) [11]. In this case the overall lattice incompressibility screens the direct effect of pressure in the Cu-O bonds.

In a first run up to 3.55 GPa it was found that at higher pressures the quality of the single crystal deteriorated using the hydrostatic medium methanol-ethanol even though the indexation showed a drastic change in the lattice parameters consistent with a phase transition. In order to solve the structure of the high-pressure phase we repeated the experiment but this time using parabar. So we went to 3.52 GPa and this time the quality of the crystal allowed us to solve its structure. It was found that the high-pressure phase presents a monoclinic structure as explained above (Fig. 1) which is described in space group $P2_1/c$. In fact, in Fig. 1 it can be observed in red how the high-pressure phase is built from the low-pressure phase. A tilt of 90° of the gunidinium complexes and the alignment of all the long Cu-O bonds induces a distortion to the lattice with a monoclinic angle of 104.44(17)°. In order to understand what produces this phase transition we

need to look at the evolution of the Cu-O distances and in particular to the JT distortion presented in Fig. 4 (b). When the phase transition takes place at 3.52 GPa, the long Cu-O bond distances abruptly increase from 2.24 $\AA$ to 2.33 $\AA$ while the short distances remain almost constant. This translates into an increase of the JT distortion from 0.33 to 0.42 $\AA$. Such a behavior under compression is regularly observed in compounds presenting non diluted Cu^{2+} [4, 11]. The JT distortion is reduced upon pressure until it reaches a critical value which approximates to 0.3 $\AA$. At that point the system finds an easy structural distortion which in this case consists on a 90° tilt of the guanidinium complexes needed to accommodate all the JT distorted axes of the CuO_6 polyhedra along the [100] direction. Furthermore, the rotation in the phase transition of all the CuO_6 polyhedra to point towards the [100] direction (Fig. 1) serves to introduce a center of inversion into the high-pressure structure.

4 Conclusions

The solution by means of single crystal x-ray diffraction of the structure of $[C(NH_2)_3]Cu(HCOO)_3$ at different pressures has provided information about the influence that the Jahn-Teller distortion of the CuO_6 polyhedra has on the stability of this structure. It has been found that $[C(NH_2)_3]Cu(HCOO)_3$ undergoes a structural phase transition ($Pna2_1 \hookrightarrow P2_1/c$) at 3.52 GPa as a consequence of the Jahn-Teller distortion σ_{JT} when it reaches a minimum critical value of 0.32 $\AA$. If we compare the minimum critical σ_{JT} found in this work with those found in other organic and inorganic systems before the occurrence of a phase transition (0.32 $\AA$ in $CuWO_4$ at 8.5 GPa) and (0.28 $\AA$ in $[(CH_3)_2NH_2]Cu(HCOO)_3$ at 7.15 GPa) one can conclude that the critical Cu^{2+} Jahn-Teller distortion in CuO_6 polyhedra before the occurrence of a phase transition is normally around 0.3 $\AA$ independently of the bearing matrix.

Acknowledgments

We thank the Servicios Generales de Apoyo a la Investigación (SEGAI) at La Laguna University and Dr. González-Platas for the single-crystal x-ray diffraction measurements. We also thank Dr. Eiken Hassühl from the Goethe Universität Frankfurt (Germany) for providing the samples. The Spanish MCIN is acknowledged for providing funding through the I+D+i project PID2021-125927NA-C22 (MCIN/AEI/10.13039/501100011033).

We would also like to express our gratitude to the Real Sociedad Española de Física for giving us the opportunity to do this project. On my part, I would like to thank my tutor, Javier Ruiz Fuertes, whose guidance and support have been essential for the development of this work.

References

[1] Xu, G.-C., Zhang, W., Ma, X.-M., Chen, Y.-H., Zhang, L., Cai, H.-L., Wang, Z.-M., Xiong, R.-G., & Gao, S. (2011). *Journal of the American Chemical Society*, 133(38), 14948–14951.

[2] Mączka, M., Ciupa, A., Gagor, A., Sieradzki, A., Pikul, A., & Ptak, M. (2016). *Journal of Materials Chemistry C*, 4(6), 1186–1193.

[3] Scatena, R., Andrzejewski, M., Johnson, R. D., & Macchi, P. (2021). *J. Mater. Chem. C*, 9(25), 8051–8056.

[4] Collings, I. E., Bykov, M., Bykova, E., Hanfland, M., van Smaalen, S., Dubrovinsky, L., & Dubrovinskaia, N. (2018). *CrystEngComm*, 20(25), 3512–3521.

[5] Hu, K.-L., Zhao, Y., Wang, S., Zhang, Y., & Li, Z. (2009). *Chemistry – A European Journal*, 15(44), 12050–12064.

[6] Agilent Technologies. (2016). CrysAlisPro Software. Agilent Technologies.

[7] Sheldrick, G. M. (2015). SHELXL-2014/7: Program for the Solution and Refinement of Crystal Structures. University of Göttingen.

[8] Silvera, I. F., Chijioke, A. D., Nellis, W. J., Soldatov, A., & Tempere, J. (2007). *Physica Status Solidi (b)*, 244(1), 460–467.

[9] Birch, F. (1947). *Physical Review*, 71(11), 809–824.

[10] Murnaghan, F. D. (1944). *Proceedings of the National Academy of Sciences of the United States of America*, 30(9), 244–247.

[11] Ruiz-Fuertes, J., Friedrich, A., Pellicer-Porres, J., Errandonea, D., Segura, A., Morgenroth, W., Haussühl, E., Tu, C.-Y., & Polian, A. (2011). *Chemistry of Materials*, 23(18), 4220-4226.